

Supplementary Information

Title: Zinc²⁺ ion inhibits SARS-CoV-2 main protease and viral replication *in vitro*.

Authors: Love Panchariya^{1†}, Wajahat Ali Khan^{1†}, Shobhan Kuila^{1†}, Kirtishila Sonkar¹, Sibasis Sahoo¹, Archita Ghoshal¹, Ankit Kumar², Dileep Kumar Verma², Abdul Hasan², Shubhashis Das³, Jitendra K Thakur³, Rajkumar Halder⁴, Sujatha Sunil², Arulandu Arockiasamy^{1*}

Affiliation:

¹Membrane Protein Biology Group, International Centre for Genetic Engineering and Biotechnology, Aruna Asaf Ali Marg, New Delhi-110067. India.

²Vector Borne Diseases Group, International Centre for Genetic Engineering and Biotechnology, Aruna Asaf Ali Marg, New Delhi-110067. India.

³Plant Mediator Lab, National Institute of Plant Genome Research, Aruna Asaf Ali Marg, New Delhi- 110 067

⁴Ruhvenile Biomedical OPC PVT LTD, Plot No-8, OCF Pocket Institution, Sarita Vihar, New Delhi-110070. India.

[†]These authors contributed equally to the work presented.

For correspondence:

*Correspondence should be addressed to: sam@icgeb.res.in / asamy001@gmail.com

Communicating author:

Arockiasamy Arulandu

International Centre for Genetic Engineering and Biotechnology (ICGEB),

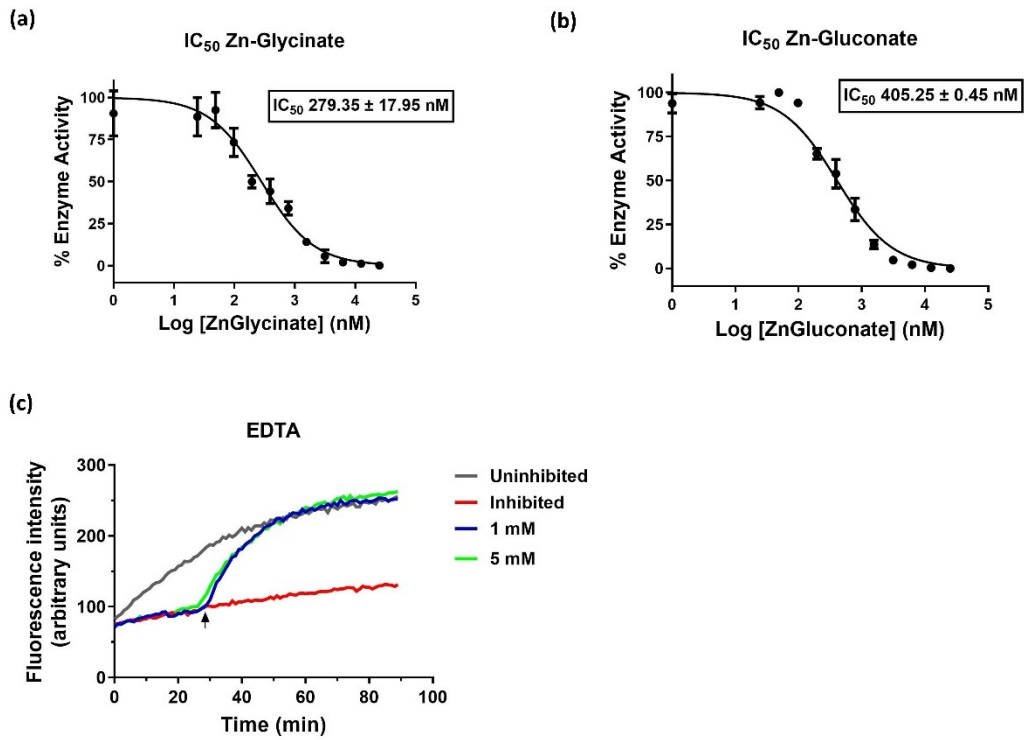
Aruna Asaf Ali Marg,

New Delhi 110067. India.

Phone: +91-11-26741358 Ext-172

Fax: +91-11-26742316

Mobile: +91-9711055502

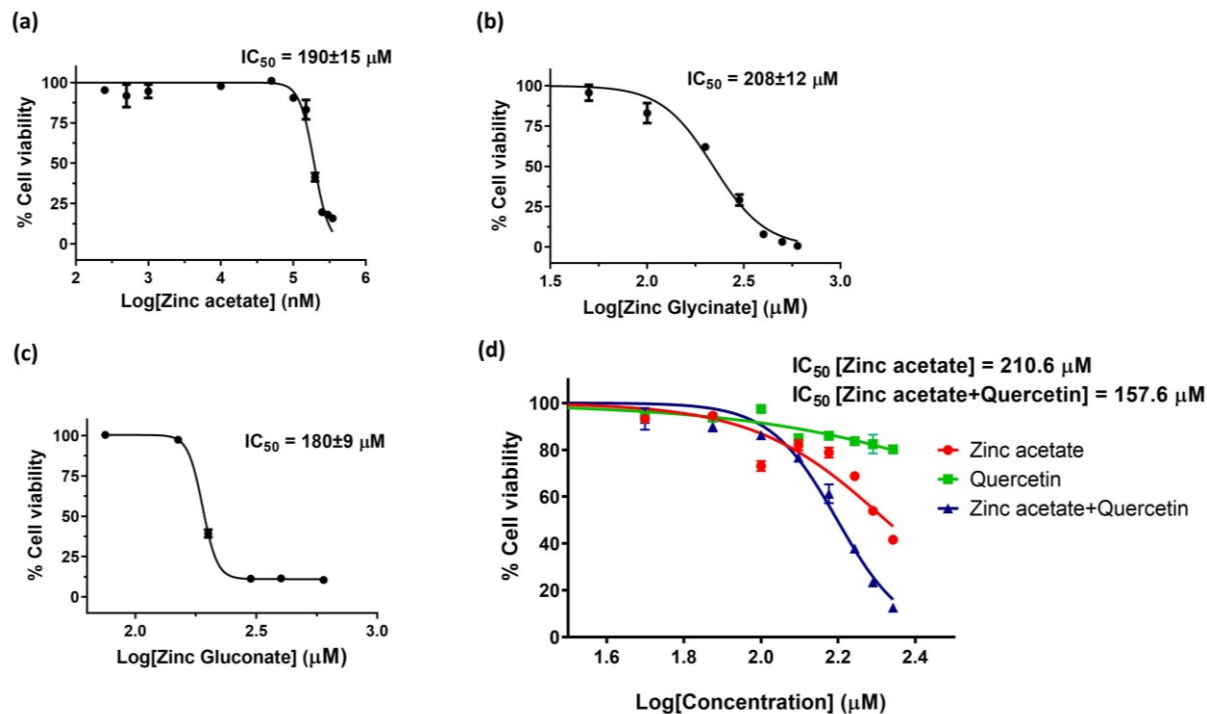


26

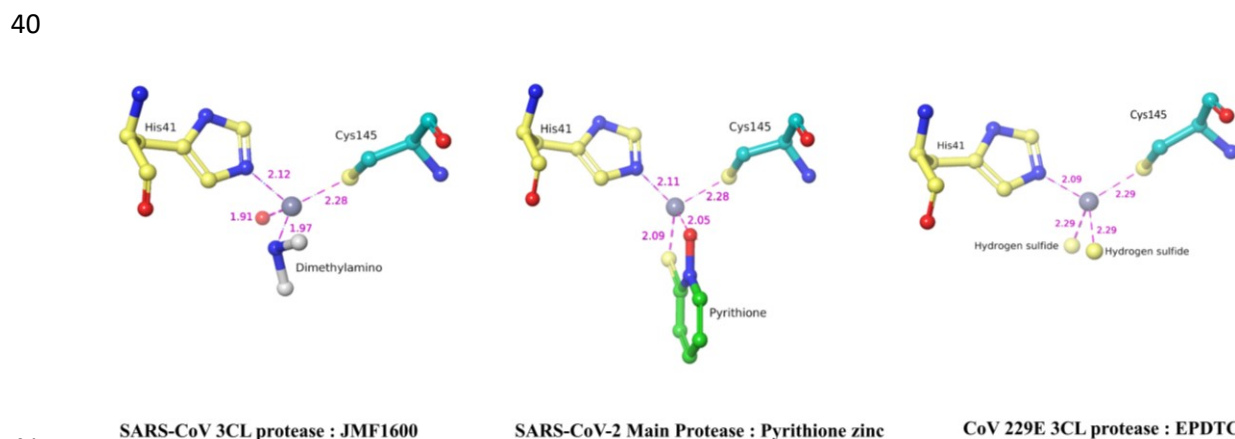
27

28 **Supplementary Figure 1. Mpro Inhibition by Zn-complexes.** IC₅₀ and concentration
 29 dependent inhibition of Mpro by zinc-Glycinate (a) and Zinc-Gluconate (b), respectively. (c)
 30 Inhibition with 500 nM Zinc acetate was completely reversed by the addition of 1 and 5 mM of
 31 EDTA at the 28th minute of the ongoing enzymatic reaction.

32



33
 34 **Supplementary Figure 2. Toxicity determination of Zinc and its complexes in Vero E6 cells.**
 35 Non-toxic concentrations were determined by studying the effect of Zinc acetate (a), Zinc
 36 glycinate (b), and Zinc gluconate (c) on the proliferation of Vero E6 cells after 48 h post
 37 addition, as determined by MTT assays. (d) Non-toxic concentrations for Zinc acetate and
 38 quercetin (1:1 molar mixture, blue) is compared with Zinc acetate alone (red). IC₅₀ for quercetin
 39 alone (green) could not be determined. All experiments are done in biological triplicates.



42 **Supplementary Figure 3: Metal ion coordination of Zinc-complexes bound to coronavirus**
 43 **3C-like proteases.** Ball and stick model representation of 3CL-pro-Zn complex crystal
 44 structures; SARS-CoV-Mpro-JMF1600 (PDB: 2Z9K), SARS-CoV-2-Mpro-Zn-pyrithione (PDB:
 45 7B83) and HCoV-229E-3CLpro-N-ethyl-n-phenyl-dithiocarbamic acid (EPDTC) (PDB: 2ZU2).
 46 Zinc is depicted as grey ball. Interatomic distances are represented as dotted lines with bond
 47 distance in angstrom (Å).

Experiment	ka (1/Ms)	kd (1/s)	KD (M)	Rmax (RU)	Chi ² (RU ²)	U-value
1	8960	0.01745	1.95E-06	57.32	3.39	2
2	8899	0.01765	1.98E-06	57.58	3.36	3
Median	8,930±30	0.01755±1 0	1.965E-06 ±0.15E-07	57.45±0.13	3.375±0.015	2.5±0.5

48

49 **Supplementary Table 1. Binding kinetics of Zinc²⁺ and SARS-CoV-2 Mpro.** Using 1:1
50 binding model, association [ka (1/Ms)] and dissociation [KD (1/s)] rate constants, and affinity
51 [KD (M)] are shown. The goodness of fit (Chi² = 3.375±0.015) is within the suggested 10% of
52 the Rmax (57.45±0.13). U-values of 2 and 3 reflect 98 and 97% confidence in KD value
53 respectively. The affinity (KD) of Zinc²⁺ for Mpro is ~2 μM. The experiment was repeated twice
54 to get the median KD of 1.96 μM.

55

	Mpro-Zn (PDB:7DK1)	Mpro-Apo (control)
Data collection		
Space group	P 21 21 21	P 21 21 21
Cell dimensions		
<i>a, b, c</i> (Å)	67.6, 102.2, 102.3	67.7, 100.7, 104.0
α, β, γ (°)	90, 90, 90	90, 90, 90
<i>R</i> _{merge}	0.09	0.086
Resolution (Å)	72.32 – 1.90	56.79 – 1.81
<i>I</i> / σI	2.69 (1.9)	2.44 (1.8)
Completeness (%)	100.0	100.0
Redundancy	12.8	12.8
Refinement		
Resolution (Å)	72.32 – 1.90	56.79 – 1.81
No. reflections	56,431	66,014
<i>R</i> _{work} / <i>R</i> _{free}	0.191/ 0.213	0.187/0.216
No. atoms		
Protein	4,582	4,649
Ligand/ion	40	38
Water	423	617
<i>B</i> -factors		
Protein	32.4	29.4
Zinc ion	40.75	-
R.m.s. deviations		
Bond lengths (Å)	0.41	0.39
Bond angles (°)	0.58	0.58

56

57 **Supplementary Table 2. X-ray data processing and refinement statistics.** The data given is
58 for SARS-CoV-2 Apo-Mpro and Mpro-Zn complex crystals, both crystallized in the same
59 condition.

60

61 **Materials and methods:**

62 **SARS-CoV-2 Mpro purification:** *E. coli* overexpression plasmid pGEX-6p-1 containing
63 SARS-CoV-2 Mpro was a kind gift from Rolf Hilgenfeld, Institute of Biochemistry, University
64 of Lübeck, Lübeck, Germany ^{1,2}. The procured construct is designed to generate authentic N
65 terminus by auto-proteolytic cleavage via Mpro at the cleavage-site SAVLQ↓SGFRK (arrow
66 represents the cleavage site). Authentic C-terminus was generated by cleaving the C-terminus 6X
67 His-tag at SGVTFQ↓GP by HRV3C protease.

68

69 Overexpression and protein purification were performed according to a previous report² with
70 some modifications. Expression plasmid was transformed into *E. coli* BL21 (DE3). Transformed
71 cells were inoculated into 200 mL LB media (Luria Bertani Broth, Miller, Himedia)
72 supplemented with ampicillin (100 µg/mL) and grown at 37 °C for 3 h at 100 RPM. The primary
73 culture was used to inoculate 6 L of LB media supplemented with ampicillin and induced with
74 0.5 mM of isopropyl-D-thiogalactoside (IPTG) after OD₆₀₀ reached 0.8 at 37 °C. 5 h post
75 induction at 37 °C, cells were harvested by centrifugation at 4000 RPM for 20 min at 4 °C and
76 stored at -20 °C until further use. The frozen cell pellet was resuspended in lysis buffer (20 mM
77 Tris, 150 mM NaCl, 10 mM imidazole, 10 µg/ml DNase-I, 100 µg/ml Lysozyme, pH 7.8) and
78 subjected to lysis by sonication on ice, followed by centrifugation at 13000 RPM for 50 min at 4
79 °C. The supernatant was loaded onto serially connected 2x 5ml HisTrap FF columns (GE) at 0.5
80 ml/min flow rate, pre-equilibrated with buffer A (20 mM Tris, 150 mM NaCl, 10 mM Imidazole
81 pH 7.8). Non-specifically bound proteins were removed by washing with 5 column volumes
82 (CV) of buffer A. The bound proteins were eluted using buffer B (20 mM Tris, 150 mM NaCl,
83 500 mM imidazole, pH 7.8) with a linear gradient of 10 to 500 mM imidazole. Fractions
84 containing Mpro were pooled and concentration was estimated using OD₂₈₀³. At this stage,
85 many contaminant proteins were observed. To cleave the C-terminal His-tag, HRV3C⁴ protease
86 was mixed with SARS-CoV-2 Mpro in 1:5 ratio (mg/mg) and dialysed into buffer C (20 mM
87 Tris, 150 mM NaCl, 1 mM DTT, pH 7.8) overnight at 4 °C. This was followed by one more
88 round of dialysis for 6 h in buffer A to remove DTT. Dialysed and tag-cleaved protein was
89 passed through serially connected 2x 5ml HisTrap FF columns. Flow through containing
90 enriched Mpro was collected and buffer exchanged with buffer D (20 mM Tris, 1 mM DTT, pH

91 8.0) using a HiPrep 26/10 desalting column (GE). Desalted protein was loaded onto 5 ml HiTrap
92 Q HP column (GE) pre-equilibrated with buffer D, and eluted using a linear gradient of 0 to 500
93 mM NaCl in 20 CV of buffer E (20 mM Tris, 1 M NaCl, 1 mM DTT, pH 8.0). Fractions
94 containing pure Mpro were pooled, concentrated and further purified with gel filtration
95 chromatography using pre-equilibrated HiLoad 16/600 Superdex 75 pg column with buffer C at
96 a flow rate of 1 ml/min. Purified protein was concentrated to 27.5 mg/ml, aliquoted and flash
97 frozen in liquid nitrogen and stored at -80 °C until further use.

98 **Surface Plasmon Resonance (SPR):** Experiments were performed using Biacore T200 with
99 control software V2.0 and Evaluation Software V3.1 (GE Life Sciences). All measurements
100 were made at 25 °C. Running buffer consisted of HBS-N pH 7.4 (10 mM HEPES, 150 mM
101 NaCl, pH adjusted with NaOH). Purified Mpro was immobilized onto a CM5 chip using amine
102 coupling method according to manufacturer's protocols with 420 s of surface activation with
103 freshly prepared 1:1 mixture of 1-ethyl-3-(3-dimethylaminopropyl) carbodiimide hydrochloride
104 (EDC) and N-hydroxysuccinimide (NHS) followed by 420 s contact time for the protein over the
105 activated surface at a flow rate of 10 µl/min. The protein (50 µg/ml) was immobilized onto the
106 chip surface in 10 mM acetate buffer pH 4.0 achieving an RU of ~14000. The remaining
107 activated carboxy methyl groups on the surface were blocked by an injection of 1 M-
108 ethanolamine-HCl pH 8.5 for 7 min. An unmodified flow cell surface was used as a reference for
109 each analysis to check for the non-specific binding response to dextran matrix. Running buffer
110 containing varying concentrations of Zinc acetate; 156 nM to 10 µM, were prepared and passed
111 over the immobilized protein at a constant flow rate of 30 µL/min. The interaction (association
112 time 60 s and dissociation time 120 s) between the protein and the analyte resulted in
113 characteristic sensorgrams which were then analysed using Biacore T200 evaluation software;
114 responses generated from unmodified surface were subtracted from the same. The curves
115 (sensorgrams) were fitted using 1:1 model to get the association rate [ka (1/Ms)], dissociation
116 rate [kd (1/s)], and equilibrium dissociation constant [KD (M)] for the interaction. The
117 regeneration was done using 50 mM NaOH, 1 M NaCl solution with 30 s contact time at 30
118 µL/min flow rate. The experiments were repeated twice to get the median values.

119

120 **Mpro enzyme inhibition assay:** Inhibitory roles of Zinc²⁺ on enzyme activity were tested via
121 FRET-based enzyme assay⁵. Fluorogenic peptide substrate (Dabcyl)-KTSAVLQ↓SGFRKM-E
122 (Edans)-NH₂; (GL Biochem) contains the cleavage site of SARS-COV-2 Mpro (cleavage site
123 represented by ↓). Cleavage of the peptide is marked with an increase in fluorescence from
124 EDANS, which was monitored with microplate reader (Spectramax M3, Molecular devices) at
125 360 nm excitation and 460 nm emission wavelengths.

126 As DTT chelates Zinc ions, SARS-COV-2 Mpro was buffer exchanged into reaction buffer (20
127 mM Tris, 100 mM NaCl, 0.5 mM TCEP, pH 7.3) using PD SpinTrap G-25 column (GE) to
128 remove DTT. 5 μL of Mpro at a final concentration of 200 nM was added to 35 μL pre pipetted
129 reaction buffer in a black 96 well plate. For IC₅₀ calculation, 5 μL inhibitor at concentrations
130 ranging from 25 μM to 12.2 nM (2-fold serial dilution), was added to the protein-containing
131 reaction mixture and incubated at 25°C for 30 min with gentle shaking. The reaction was started
132 by adding 5 μL substrate at a final concentration of 20 μM, immediately after which the relative
133 fluorescence was read for 45 min. The total reaction volume was 50 μL. Data were normalized
134 by considering negative control (protein heat inactivated at 60° C for 5 min) as 100% inhibition
135 while treating positive control as 0% inhibition.

136 To test reversibility of Zinc²⁺ inhibition, 200 nM protein was first incubated with 500 nM zinc
137 acetate for 30 min at 25° C with gentle shaking as described above. The reaction was then
138 initiated with 20 μM substrate. 1 and 5 mM EDTA were added in separate wells at 28th minute
139 when the reading was being taken.

140

141 **SARS-CoV-2 Mpro crystallization and soaking with Zinc:** Purified protein was diluted to
142 13.6 mg/ml for crystallization in buffer C. Several flower-like multi-crystals were obtained after
143 overnight incubation at 20° C in the reservoir solution containing 100 mM Bis-Tris, 20% PEG
144 3350 and 5% DMSO pH 6.5⁶. These multi-crystals were used to prepare seeds using seed beads
145 (Hampton research). Seeding was done into 3 μL protein: reservoir (2:1) drop in a 24 well sitting
146 drop plate (Hampton research). Thereafter, single crystals with thin plate-like morphology were
147 obtained after overnight incubation. Reservoir containing 10 mM Zinc glycinate or Zinc
148 gluconate (TCI chemicals #G0215 and #G0277, respectively) was added to wells containing
149 good quality crystals and soaked for 4 h. Crystals were then fished out and cryo-protected in a

150 solution containing the reservoir with 20% glycerol. Subsequently, crystals were immediately
151 flash-frozen into liquid nitrogen and stored for further X-ray diffraction and data collection.
152 Multiple attempts to co-crystallize with zinc salts failed due to heavy precipitation of the protein.
153 Also, soaking solutions containing Zinc²⁺ such as Zinc acetate or Zinc sulphate deteriorated the
154 crystal quality.

155

156 **X-ray data collection, processing and refinement:** X-ray diffraction data for Zinc-soaked
157 SARS-CoV-2 Mpro crystals were collected at XRD2 beamline⁷, Elettra Sincrotrone Trieste at
158 0.99Å wavelength on a Dectris Pilatus 6M detector. Collected data were processed with
159 autoPROC⁸ and structure was determined by molecular replacement using Phaser-MR of Phenix
160 crystallographic suite⁹ using 6Y2F as search template. Initial model building was done with
161 AutoBuild¹⁰ module. Structure and map quality were further improved by manual building with
162 Coot¹¹ and refinement with autoBUSTER¹². Refinement statistics are summarised in
163 Supplementary Table 2. Final model has R_{work} and R_{free} of 0.19 and 0.21 respectively. The
164 structure has no Ramachandran outliers and 0.8 % side chain outliers. Figures were made with
165 UCSF Chimera¹³ and Maestro, Schrodinger suite¹⁴ (Licenced to ICGEB).

166

167 **Molecular Dynamics:** Crystal structure of SARS-CoV-2 Mpro with Zinc (PDB: 7DK1) was
168 prepared with protein preparation wizard of Schrodinger suite. Protonation states at pH 7.4±0.5
169 were created for the complex, explicit hydrogens were added to the structure, and zero bond
170 order was created for Zinc²⁺ ion. Hydrogen bond optimization was done with ProtAssign and
171 finally restrained minimization was performed using OPLS3e force field to obtain input structure
172 for further calculations and analysis before performing Molecular Dynamic (MD) simulations.

173 To analyse the stability of the SARS-CoV-2 Mpro-Zinc complex, a 1 µs MD simulation was
174 performed using Desmond¹⁵ (Schrodinger) and the coordinates were saved at an interval of 50
175 ps. Simulation system was built using OPLS3e force field and solvated with TIP3P water model.
176 Orthorhombic box with an edge length of 10 Å was set, ensuring a minimal distance between the
177 atoms of protein complex and edge of the box. Counter ions were added to neutralize the system;
178 further, 0.15 M NaCl was added to the solvated box as salt. The prepared systems were relaxed

179 before the actual simulation by a series of energy minimization and short MD simulations, which
180 mainly comprise of six relaxation steps while keeping the solute restrained. Briefly, in the first
181 two steps, systems were relaxed with Brownian Dynamics NVT at T=10 K for 100 ps and 12 ps
182 respectively. In step 3 and 4, NPT equilibration was done for 12 ps at 10 K with restrains on
183 heavy solute atoms. At step 5, the pocket was solvated. Finally, in step 6 and 7 short NPT
184 equilibrations were done for 12 and 24 ps respectively. The NPT ensemble was employed for the
185 simulations with Nose-Hover chain thermostat and the Maryna-Tobias-Klein barostat. RESPA
186 integrate was used with a time step of 2 fs. For short range of coulombic interactions, a 9 Å cut
187 off was considered. Analysis of the simulation was done with simulation event analysis,
188 Desmond.

189

190 **Cell culture and virus strain:** Vero E6 cells (African green monkey kidney cells) were
191 purchased from ATCC, grown and maintained in Minimal Essential Media (MEM; HIMEDIA;
192 AL047S) supplemented with 10 % FBS (HIMEDIA, RM10681), 2 mM L-Glutamine
193 (HIMEDIA; TCL012), 100 U/ml penicillin, and 10 mg/ml streptomycin, in a 5 % carbon dioxide
194 incubator with controlled humidity at 37 °C. For antiviral studies, SARS-CoV-2 strain, USA-
195 WA1/2020 was used. All the virus infection and subsequent experiments using virus were
196 performed in BSL-3 (virology) facility at ICGEB, New Delhi.

197

198 **Cell viability assay:** Cytotoxicity of Zinc acetate, Zinc glycinate, and Zinc gluconate on the
199 viability and proliferation of the Vero E6 cells was evaluated using MTT assay. Cells were
200 seeded at a density of 7000 cells per well in a 96-well plate. After allowing the cells to attach
201 overnight, they were treated with varying concentrations of the above compounds. Treatment
202 was done in MEM supplemented with 2% FBS for 48 h, at the end of which MTT assay was
203 performed as per manufacturer's protocol. GraphPad Prism software was used to determine the
204 IC₅₀ (50% inhibitory concentration). The absorbance (A) was measured at 570 nm and the
205 percentage cell viability was calculated using the following formula:

206 $\text{Percentage cell viability} = (A_{570} \text{ of treated}) / A_{570} \text{ of Untreated} * 100$

207

208 **Anti-SARS-CoV-2 assay:** Anti-viral assays with Zinc acetate, Zinc gluconate, Zinc glycinate
209 and Zinc acetate: quercetin mixture (1:2 molar ratio) were performed using a standard assay
210 reported for SARS-CoV-2 and other viruses^{16,17}. Vero E6 cells were seeded in 24-well plates, a
211 day prior to infection. The following day, Zinc and other compounds were added to these seeded
212 cells at maximum non-toxic concentration (100 μ M, 70 μ M and 100 μ M respectively) followed
213 by infection with SARS-COV-2 (Multiplicity of infection; MOI= 0.1). The treated and virus
214 infected cells were incubated for 48 h (37 °C, 5% CO₂) following which the supernatants were
215 harvested for viral quantification by plaque assay and qRT-PCR.

216

217 **Plaque assay:** For viral quantification, Vero E6 cells were seeded in 96 well plates, followed by
218 viral inoculation on the next day using dilutions; starting at 1:50 the virus was double diluted till
219 1:51200. The virus was incubated with the cells for 2 h at 37 °C for viral adsorption. Thereafter,
220 the media containing the inoculum was removed, and wells were overlaid with 150 μ L of 1%
221 carboxymethylcellulose (CMC) prepared in MEM media (containing 10% FBS). The plates were
222 then incubated at 37 °C for 96 h with 5% CO₂ and 75% humidity. Post incubation, the cells were
223 fixed with 5% formaldehyde before washing twice with 1 \times PBS and staining was performed
224 using 0.25% crystal violet (prepared in 30% methanol). Plaques were visualized and counted to
225 calculate viral titers using the following formula:

226
$$\text{Plaque forming units (pfu)} = (\text{No. of plaques}) / (\text{Dilution} \times \text{volume of virus})$$

227

228 **qRT-PCR:** To quantify the viral RNA using qRT-PCR, 150 μ L media from the treated,
229 untreated and virus infected wells was collected, and used for RNA isolation using the
230 NucleoSpin Viral RNA isolation kit (740956.250). Isolated RNA samples were then subjected to
231 One-step qRT-PCR using QuantiTect qRT-PCR kit (Qiagen #1054498) and PIKOREAL 96
232 Real-Time PCR system (Thermo scientific). Data analysis was performed using a standard curve
233 to calculate genome equivalents of SARS-CoV-2 in all the samples.

234

235 **References:**

- 236 1 Wu, F. *et al.* A new coronavirus associated with human respiratory disease in China. *Nature* **579**,
237 265-269, doi:10.1038/s41586-020-2008-3
- 238 10.1038/s41586-020-2008-3 [pii] (2020).
- 239 2 Hilgenfeld, R. From SARS to MERS: crystallographic studies on coronaviral proteases enable
240 antiviral drug design. *FEBS Journal* **281**, 4085-4096, doi:10.1111/febs.12936 (2014).
- 241 3 Pace, C. N., Vajdos, F., Fee, L., Grimsley, G. & Gray, T. How to measure and predict the molar
242 absorption coefficient of a protein. *Protein Sci* **4**, 2411-2423, doi:10.1002/pro.5560041120
243 (1995).
- 244 4 Raran-Kurussi, S. & Waugh, D. S. A dual protease approach for expression and affinity
245 purification of recombinant proteins. *Anal Biochem* **504**, 30-37, doi:10.1016/j.ab.2016.04.006
- 246 S0003-2697(16)30029-X [pii] (2016).
- 247 5 Kao, R. Y. *et al.* Characterization of SARS-CoV main protease and identification of biologically
248 active small molecule inhibitors using a continuous fluorescence-based assay. *FEBS Lett* **576**,
249 325-330, doi:S0014579304011421 [pii]
- 250 10.1016/j.febslet.2004.09.026 (2004).
- 251 6 Kneller, D. W. *et al.* Structural plasticity of SARS-CoV-2 3CL M(pro) active site cavity revealed by
252 room temperature X-ray crystallography. *Nat Commun* **11**, 3202, doi:10.1038/s41467-020-
253 16954-7
- 254 10.1038/s41467-020-16954-7 [pii] (2020).
- 255 7 Lausi, A. *et al.* Status of the crystallography beamlines at Elettra. *The European Physical Journal*
256 *Plus* **130**, 43, doi:10.1140/epjp/i2015-15043-3 (2015).
- 257 8 Vonrhein, C. *et al.* Data processing and analysis with the autoPROC toolbox. *Acta Crystallogr D*
258 *Biol Crystallogr* **67**, 293-302, doi:10.1107/S0907444911007773
- 259 S0907444911007773 [pii] (2011).
- 260 9 Liebschner, D. *et al.* Macromolecular structure determination using X-rays, neutrons and
261 electrons: recent developments in Phenix. *Acta Crystallogr D Struct Biol* **75**, 861-877,
262 doi:10.1107/S2059798319011471
- 263 S2059798319011471 [pii] (2019).
- 264 10 Terwilliger, T. C. *et al.* Iterative model building, structure refinement and density modification
265 with the PHENIX AutoBuild wizard. *Acta Crystallogr D Biol Crystallogr* **64**, 61-69,
266 doi:S090744490705024X [pii]
- 267 10.1107/S090744490705024X (2008).
- 268 11 Emsley, P., Lohkamp, B., Scott, W. G. & Cowtan, K. Features and development of Coot. *Acta*
269 *Crystallogr D Biol Crystallogr* **66**, 486-501, doi:10.1107/S0907444910007493
- 270 S0907444910007493 [pii] (2010).
- 271 12 Buster Version 2.11.2 (2017).
- 272 13 Pettersen, E. F. *et al.* UCSF Chimera--a visualization system for exploratory research and analysis.
273 *J Comput Chem* **25**, 1605-1612, doi:10.1002/jcc.20084 (2004).
- 274 14 Schrödinger Release 2021-2: Maestro, Schrödinger, LLC. (2021).
- 275 15 Phillips, J. C. *et al.* Scalable molecular dynamics with NAMD. *J Comput Chem* **26**, 1781-1802,
276 doi:10.1002/jcc.20289 (2005).

277 16 Caly, L., Druce, J. D., Catton, M. G., Jans, D. A. & Wagstaff, K. M. The FDA-approved drug
278 ivermectin inhibits the replication of SARS-CoV-2 in vitro. *Antiviral Res* **178**, 104787, doi:S0166-
279 3542(20)30201-1 [pii]
280 10.1016/j.antiviral.2020.104787 (2020).
281 17 Kalita, P., Padhi, A. K., Zhang, K. Y. J. & Tripathi, T. Design of a peptide-based subunit vaccine
282 against novel coronavirus SARS-CoV-2. *Microb Pathog* **145**, 104236, doi:S0882-4010(20)30523-4
283 [pii]
284 10.1016/j.micpath.2020.104236 (2020).
285
286